

Boundary scattering in the ϕ^4 model

Patrick Dorey[†], Aliaksei Halavanau^{*}, James Mercer[†], Tomasz Romanczukiewicz[‡] and Yasha Shnir^{*§¶}

[†]*Department of Mathematical Sciences, Durham University, UK*

^{*}*Belarusian State University, Minsk, Belarus*

[‡]*Inst. of Physics, Jagiellonian University, Krakow, Poland*

[§]*BLTP, JINR, Dubna, Russia*

[¶]*Inst. of Physics, Oldenburg University, Germany*

(Dated: August 11, 2015)

We study boundary scattering in the ϕ^4 model on a half-line with a one-parameter family of Neumann-type boundary conditions. A rich variety of phenomena is observed, which extends previously-studied behaviour on the full line to include regimes of near-elastic scattering, the restoration of a missing scattering window, and the creation of a kink or oscillon through the collision-induced decay of a metastable boundary state.

PACS numbers: 11.10.Lm, 11.27.+d

Introduction. Systems with boundaries, defects and impurities have been intensively studied in statistical physics and field theory, both at the classical and the quantum levels. Often the key physics of the model can be captured, possibly after dimensional reduction, by a simple 1+1 dimensional field theory on a half line. Examples include the Kondo problem [1], fluxon propagation in long Josephson junctions [2], the XXZ model with boundary magnetic field [3], an impurity in an interacting electron gas [4], the sine-Gordon [5] and Toda [6] models, monopole catalysis [7], the Luttinger liquid [8], and a toy model motivated by M-theory [9].

Especially since the work of Ghoshal and Zamolodchikov [5], there has been great interest in boundary conditions compatible with bulk integrability, and many such models turn out to be of direct physical interest. However less attention has been paid to the equally if not more physically-relevant cases of non-integrable boundary systems, even at the classical level. This is perhaps a shame, as it is now known that non-integrable classical field theories, even in 1+1 dimensions, can exhibit remarkably rich patterns of behaviour not seen in their integrable counterparts [10–14].

In this Letter we examine the ϕ^4 theory in 1+1 dimensions, restricted to a half line by a simple Neumann-type ‘magnetic field’ boundary condition. The ϕ^4 theory on a full line is similar to the sine-Gordon model in that both support topological kinks and antikinks; the ϕ^4 theory also has an intriguing and still not fully-understood counterpart of the sine-Gordon breather, the oscillon [15]. We chose the magnetic field boundary condition in part because of its simplicity, and in part because the scattering of kinks against such a boundary provides a natural deformation of the full-line scattering problems which are already known to exhibit intricate patterns of resonant scattering [10–13]. In certain regimes our results do indeed resemble the pattern of scattering windows observed in kink-antikink collisions on the full line; in others we find novel phenomena including a new type of ‘sharp-

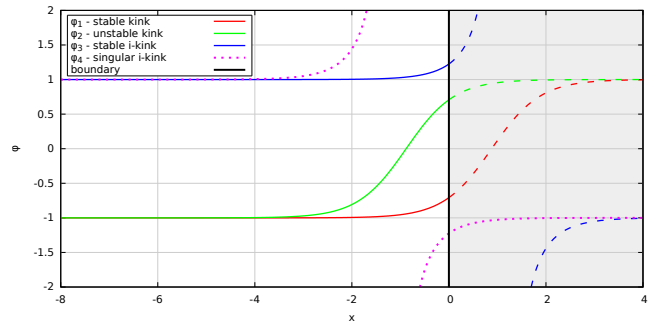


Figure 1. Static solutions for $H = 1/2$.

edged’ scattering window. Even though the theory is not integrable, it turns out to be possible to give an accurate analytical description of some aspects of this behaviour.

The model. We consider a rescaled ϕ^4 theory with vacua $\phi_v \in \{-1, +1\}$ on the left half-line $-\infty < x < 0$. The bulk energy and Lagrangian densities are $\mathcal{E} = \mathcal{T} + \mathcal{V}$ and $\mathcal{L} = \mathcal{T} - \mathcal{V}$ respectively, where

$$\mathcal{T} = \frac{1}{2}\phi_t^2 \quad \text{and} \quad \mathcal{V} = \frac{1}{2}\phi_x^2 + \frac{1}{2}(\phi^2 - 1)^2. \quad (1)$$

The static full-line kink and antikink, $\phi_K(x) = \tanh(x - x_0)$ and $\phi_{\bar{K}}(x) = -\phi_K(x)$, have rest mass $M = 4/3$ and interpolate between the two vacua. Including a boundary energy $-H\phi_0$, where $\phi_0 = \phi(0, t)$ and H can be interpreted as a boundary magnetic field, yields the Neumann-type boundary condition $\phi_x(0, t) = H$ at $x = 0$.

For $0 < H < 1$ there are four static solutions to the equations of motion, shown in Fig. 1. Two of them, $\phi_1(x) = \tanh(x - X_0)$ and $\phi_2(x) = \tanh(x + X_0)$ with $X_0 = \cosh^{-1}(1/\sqrt{|H|})$, are restrictions of regular full-line kinks to the half-line, while the other two, $\phi_3(x) = -\coth(x - X_1)$ and $\phi_4(x) = -\coth(x + X_1)$ with $X_1 = \sinh^{-1}(1/\sqrt{|H|})$ are irregular on the full line. On the half line, ϕ_3 is non-singular and corresponds to the absolute minimum of the energy, while ϕ_1 is metastable, and ϕ_2 is the unstable saddle-point between ϕ_3 and ϕ_1 . The energies can be found by rewriting

$E[\phi] = \int_{-\infty}^0 \mathcal{V} dx - H\phi_0$ in Bogomolnyi form as

$$E[\phi] = \frac{1}{2} \int_{-\infty}^0 (\phi_x \pm (\phi^2 - 1))^2 dx \mp \left[\frac{1}{3} \phi^3 - \phi \right]_{-\infty}^0 - H\phi_0. \quad (2)$$

Since ϕ_1 and ϕ_2 satisfy $\phi_x = 1 - \phi^2$ we have $\phi_1(0) = -\sqrt{1-H}$, $\phi_2(0) = \sqrt{1-H}$; while $(\phi_3)_x = \phi_3^2 - 1$ and so $\phi_3(0) = \sqrt{1+H}$. Taking the upper and lower signs in (2) as appropriate,

$$\begin{aligned} E[\phi_1] &= \frac{2}{3} - \frac{2}{3}(1-H)^{3/2}, & E[\phi_2] &= \frac{2}{3} + \frac{2}{3}(1-H)^{3/2}, \\ E[\phi_3] &= \frac{2}{3} - \frac{2}{3}(1+H)^{3/2}. \end{aligned} \quad (3)$$

As H increases through 1, ϕ_1 merges with ϕ_2 and disappears, leaving ϕ_3 as the only static solution for $H > 1$. For $H < 0$ the story is the same, with ϕ and H negated throughout, so the physically-relevant solutions are $\tilde{\phi}_i(x) = -\phi_i(x)$, $i = 1 \dots 3$.

Numerical results. We took initial conditions corresponding to an antikink at $x_0 = -10$ travelling towards the boundary with velocity $v_i > 0$. (We found the setup with an incident antikink easier to visualise, but our results apply equally to kink-boundary collisions on negating ϕ and H .) Thus the initial profile was $\phi_1(x) - \tanh(\gamma(x - x_0)) + 1$ for $H > 0$ and $\tilde{\phi}_3(x) - \tanh(\gamma(x - x_0)) + 1$ for $H < 0$, where $\gamma = 1/\sqrt{1 - v_i^2}$. Our real interest was in the problem with the initial antikink infinitely far from the boundary; the rapid decay of the antikink-boundary force (4), calculated below, meant that error in taking x_0 finite was small.

To solve the system numerically, we restricted it to an interval of length L , with the Neumann boundary condition imposed at $x = 0$ and a Dirichlet condition at $x = -L$. (Since we took run times such that radiation did not have time to reflect from the extra boundary and return, the boundary condition at $x = -L$ was anyway irrelevant.) We used a 4th order finite-difference method on a grid of $N = 1024$ nodes with $L = 100$, so the spatial step was $\delta x \approx 0.1$, and a 6th-order symplectic integrator for the time stepping function, with time step $\delta t = 0.04$. Selected runs were repeated with other values of x_0 , L , N and δt to check the stability of our results.

Our simulations revealed a rich picture, aspects of which are summarised in Figs. 2, 3. For all (H, v_i) pairs with $H < H_c \approx 0.6$, the antikink either reflects off the boundary with some velocity v_f , or becomes stuck to it – corresponding to $v_f = 0$ – to form a ‘boundary oscillon’ which then decays very slowly into radiation. At $H = 0$ (Fig. 2c) the plot of $|v_f|$ as a function of v_i reproduces the well-known structure of resonant scattering windows in $K\bar{K}$ collisions on a full line [10–12]. For *negative* values of H (Figs. 2a and b) new features emerge. For v_i small, the antikink is reflected elastically from the boundary with very little radiation. As v_i increases above a critical value v_{cr} , the antikink is trapped by the boundary, leaving only radiation in the final state. Increasing v_i further,

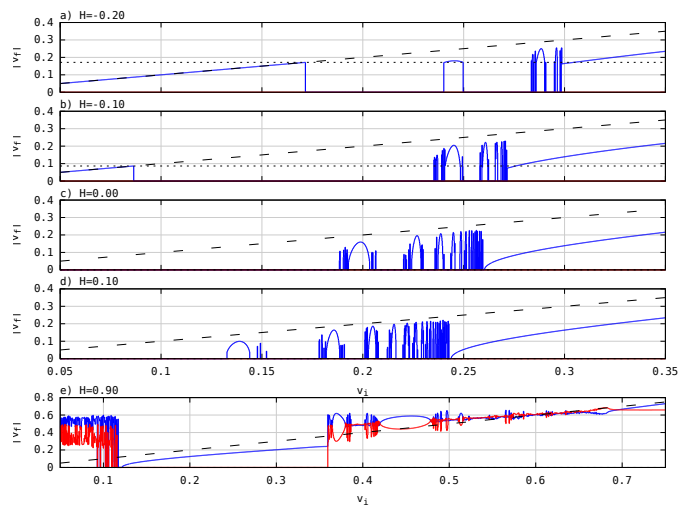


Figure 2. Final antikink velocities as functions of initial velocities. The dashed line indicates the result for a purely elastic collision. In the fifth plot, a kink can also be produced: its velocity is shown in red.

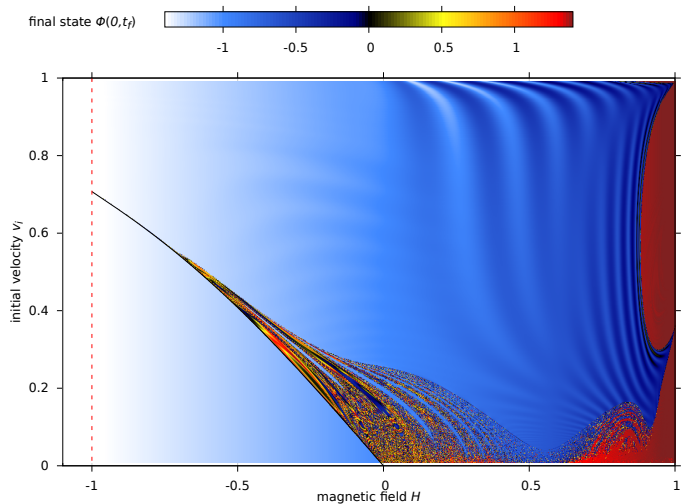


Figure 3. A ‘phase diagram’ of antikink-boundary collisions. The plot shows the value of the field at $x = 0$ a time $t_f = |x_0|/v_i + 100$ after the start of the simulation, as function of the boundary magnetic field H and the initial velocity v_i .

scattering windows begin to open, until v_i exceeds an upper critical value and the antikink again always escapes. If the antikink escapes its speed $|v_f|$ is always larger than some minimal value very slightly lower than v_{cr} , so (in contrast to the full-line situation) v_f is a discontinuous function of v_i , giving the windows the sharp edges mentioned in the introduction. For small *positive* values of H (Fig. 2d), v_f is instead a continuous function of v_i , with the sequence of windows seen at $H = 0$ shifting towards lower values of v_i while preserving its general structure. Finally, for $H > H_c$ (Fig. 2e) other new phenomena arise which have no counterparts in the full-line theory; these will be discussed further below.

Analytical considerations. To evaluate the static force between a single antikink and the boundary we place the antikink at $x = x_0 < 0$ and add a possibly-singular ‘image’ kink at $x_1 > 0$ in such a way that the combined configuration satisfies the boundary condition at $x = 0$. From the standard full-line result, the force on the antikink is equal to $32e^{-2(x_1-x_0)}$, or minus this if the image kink is singular. For $|H| \ll 1$ and $|x_0| \gg 1$ we find $e^{-2x_1} = \frac{1}{4}H + e^{2x_0}$, so

$$F = 32 \left(\frac{1}{4}H + e^{2x_0} \right) e^{2x_0}. \quad (4)$$

For $H < 0$ the force is repulsive far from the boundary, and attractive nearer in. When $x_0 = -\frac{1}{2} \log(-\frac{1}{4}H)$, $x_1 = \infty$ and the force vanishes, the antikink-kink configuration reducing to the unstable static solution $\tilde{\phi}_2$.

Now consider, also for $H < 0$, an antikink moving towards the boundary. If its velocity v_i is small, then it won’t have sufficient energy to overcome the initially-repulsive force, and it will be reflected without ever coming close to $x = 0$, and without significantly exciting any other modes; this is illustrated in Fig. 4a. Increasing v_i , at some critical value v_{cr} the energy will be just enough reach the top of the potential barrier and create the static saddle-point configuration $\tilde{\phi}_2$, as shown in Fig. 4b. The value of v_{cr} can be deduced on energetic grounds: the initial energy is $\frac{4}{3}(1 - v_{cr}^2)^{-1/2} + E[\phi_1]$, while the final energy is $E[\tilde{\phi}_2] = \frac{2}{3} + \frac{2}{3}(1+H)^{3/2}$. Equating the two,

$$v_{cr}(H) = \sqrt{1 - 4((1+H)^{3/2} + (1-H)^{3/2})^{-2}}. \quad (5)$$

If v_i is just larger than v_{cr} , the antikink can overcome the potential barrier and approach the boundary; energy is then lost to other modes and so it is unable to return, and is trapped at the boundary. Thus $v_{cr}(H)$ marks the upper limit of the windows of almost-perfectly-elastic scattering seen in Figs. 2a and 2b, and the lower edge of the ‘fractal tongue’ occupying the left half of Fig. 3. The curve $v_i = v_{cr}(H)$ is included in Fig. 3; it matches our numerical results remarkably well. Similar arguments show that, within this particle-like approximation, v_{cr} is the smallest possible speed for *any* escaping antikink, explaining the sharp (discontinuous) edges of all windows when $H < 0$.

Next we consider the perturbative sector of the model. The full-line theory has a continuum of small linear perturbations about each vacuum with mass $m = 2$; in addition a static kink $\phi_1(x) = \tanh(x - X_0)$ has a discrete normalizable mode with frequency $\omega_1 = \sqrt{3}$, and a continuum of above-threshold states $\eta(x, t) = e^{i\omega t} \eta_k(x)$ where $\omega^2 = 4 + k^2$,

$$\eta_k(x) = e^{-ikX} \left(-1 - k^2 + 3ik \tanh X + 3 \tanh^2 X \right) \quad (6)$$

and $X = x - X_0$ [17]. Considering ϕ_1 instead as a static half-line solution to the boundary theory with $0 < H < 1$,

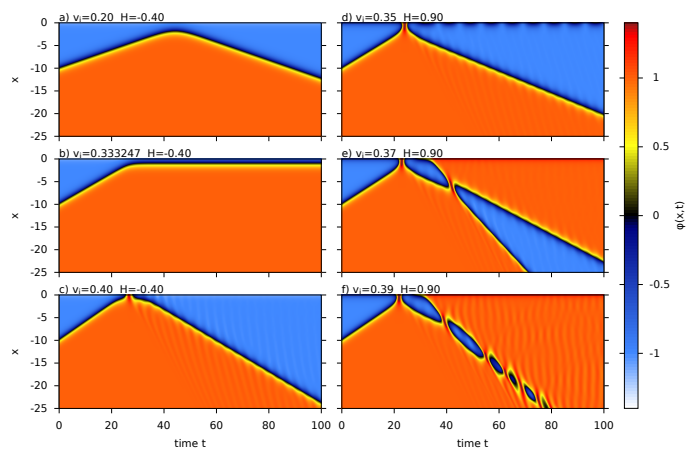


Figure 4. Example collisions for $H = -0.4$ (left) and $H = 0.9$ (right). The plots illustrate various scenarios: (a) elastic recoil at negative H and low impact velocity; (b) saddle point production, the antikink finishing on the top of the barrier; (c) single bounce; (d) single bounce with the excitation of the boundary mode; (e) kink production via collision-induced boundary decay; (f) production of a bulk oscillon.

linear perturbations must satisfy $\partial_x \eta(x) = 0$ at $x = 0$. Setting $k = i\kappa$ this yields

$$\kappa^3 - 3\phi_0 \kappa^2 + (6\phi_0^2 - 4)\kappa - 6\phi_0^3 + 6\phi_0 = 0 \quad (7)$$

where $\phi_0 = \phi_1(0) = -\sqrt{1-H}$ and now $\omega^2 = 4 - \kappa^2$. For $0 < H < 1$, $-1 < \phi_0 < 0$ and there is just one positive solution κ to Eq. (7), which furthermore satisfies $\kappa < 2$: this is a vibrational mode, localised near to the boundary. For $H < 0$, $\phi_0 < -1$, and the continuation of Eq. (7) governs the spectrum of fluctuations about $\tilde{\phi}_3(x)$, the $H < 0$ vacuum. There are no positive solutions in this regime and hence no internal modes of the boundary for $H < 0$. Finally, for $0 < \phi_0 < 1$, the equation encodes the linear perturbations of ϕ_2 , the saddle-point solution. For these cases Eq. (7) has two positive solutions but one is larger than 2: this is the unstable mode of ϕ_2 .

These results are confirmed by our simulations. Fig. 5 shows the Fourier transforms of $\phi(0, t)$ for $30 < t < 3030$, for antikink-boundary collisions with initial velocity $v_i = 0.5$, and $H = -0.1$ and 0.3 . The final velocity v_f of the reflected antikink is -0.382596 for $H = -0.1$ and -0.454014 for $H = 0.3$, so in both cases translational energy is lost to other modes during the collision.

For $H = -0.1$, the boundary does not have an internal mode, and only radiation with frequencies near to 2, the mass threshold, remains near to the boundary. The internal mode of the reflected antikink has frequency ω_1 , but this mode cannot be observed at the boundary since it is exponentially suppressed there. However nonlinear couplings with other excitations create waves with frequencies at above-threshold multiples of ω_1 [18], which can propagate to the boundary. Indeed, the upper plot of Fig. 5 shows peaks at $\Omega_1 = 2$ and $\Omega_2 = \Omega(2\omega_1)$, where $\Omega(\omega) = \gamma(\omega + k(\omega)v_f)$ is the Doppler-shifted frequency

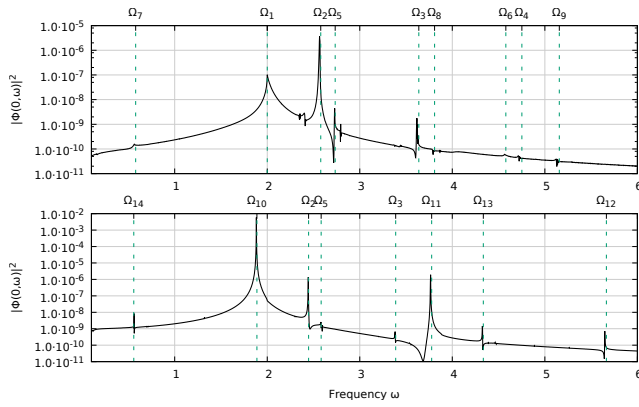


Figure 5. Power spectra at the boundary after a collision with $v_i = 0.5$, for $H = -0.1$ (upper) and $H = 0.3$ (lower).

of radiation emitted from the moving kink measured on the boundary. Higher harmonics at $\Omega_3 = \Omega(3\omega_1)$ and $\Omega_4 = \Omega(4\omega_1)$ are also visible, along with combinations of the internal mode of the antikink and the lowest continuum mode such as $\Omega_5 = \Omega(2 + \omega_1)$ and $\Omega_6 = 2 + \Omega(2\omega_1)$.

Many of these modes are also present in the $H = 0.3$ spectrum shown in the lower plot of Fig. 5, albeit at shifted locations because of the different final antikink velocity. However the plot is dominated by the internal boundary mode with frequency $\Omega_{10} = 1.888459$. The higher harmonics $\Omega_{11} = 2\Omega_{10}$ and $\Omega_{12} = 3\Omega_{10}$ are also visible, while interactions between radiation from the outgoing antikink and the boundary mode lead to peaks at $\Omega_{13} = \Omega_{10} + \Omega(2\omega_1)$ and $\Omega_{14} = \Omega_{10} - \Omega(2\omega_1)$.

Further properties. For small nonzero values of $|H|$, the resonant energy exchange mechanism governing scattering in the bulk ϕ^4 model is changed in two ways in the boundary theory: (i) The attractive force acting on the antikink near to the boundary is modified, in particular becoming repulsive at greater distances when H is negative; (ii) After the initial impact, energy can be stored not only in the internal mode of the antikink, but also, for positive values of H , in the boundary mode. These factors change the resonance condition for energy to be returned to the translational mode of the antikink on a subsequent impact, leading to the shifting (and, for negative H , sharpening) of the windows seen in Figs. 2 a-d. This return can happen after two, three or more bounces from the boundary, leading to a hierarchy of multibounce windows as in the full-line situation. However our numerical results suggest that for small positive values of H the contribution of the boundary mode in the resonant energy transfer is not significant. For larger values of $|H|$ other new features appear, two of which we now discuss.

The first is the resurrection of a ‘missing’ two-bounce window from the full-line scattering noted by Campbell et al in [10]. Fig. 2a includes a scattering window centred at $v_i \approx 0.245$ which is *not* the continuation of any of the windows seen in Figs. 2 b-d; the same window can be seen in Fig. 3 running from $(H, v_i) = (-0.12, 0.2)$ to

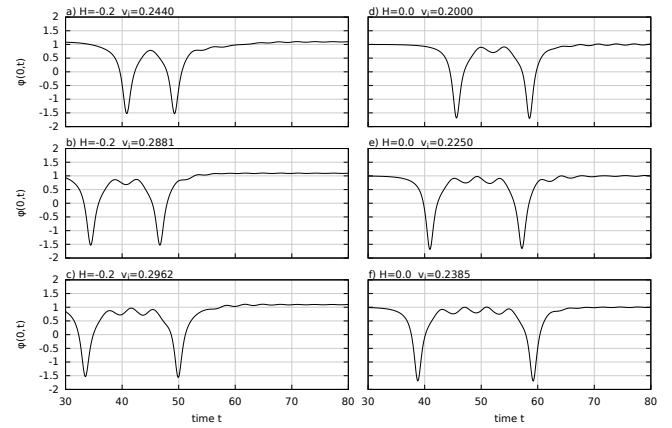


Figure 6. Plots of $\phi(0, t)$ for v_i inside the first three two-bounce windows for $H = -0.2$ (left) and $H = 0$ (right).

$(H, v_i) = (-0.45, 0.4)$. Fig. 6 plots $\phi(0, t)$ for v_i inside the first three two-bounce windows for $H = -0.2$ and $H = 0$. As explained in [10], the ‘wobbles’ between the large dips count oscillations of the internal antikink mode between bounces; as is clear from the figure, the minimum number supporting antikink escape is one smaller for $H = -0.2$ than for the full-line (equivalently, $H = 0$) case, giving rise to the extra window.

Second, for large positive values of the magnetic field the scattering can induce the metastable ϕ_1 boundary to decay to ϕ_3 with the creation of an extra kink (or sometimes a bulk oscillon) as charted in Fig. 2e, a process that has no analogue in the full-line theory. Indeed, if the boundary mode is sufficiently strongly excited by the initial antikink impact, it behaves as an intermediate state prior to the escape of a kink from the boundary, analogous to the intermediate oscillon state in the process of $K\bar{K}$ pair production on the full line [16, 18, 19]. Depending on their relative velocities, the reflected antikink and the subsequently-emitted kink may appear in the final state, or recombine to form a bulk oscillon. In Fig. 4, right panels, we show some of the processes we observed at $H = 0.90$: (d) - inelastic scattering of the antikink with excitation of the oscillon state on the boundary, (e) - production of a $K\bar{K}$ pair, (f) - production of a bulk oscillon. The region of boundary decay occupies the solid red area on the right edge of Fig. 3. An unexpected and intriguing feature is the cusp-like nick in this region terminating at $(H, v_i) \approx (1, 0.365)$. This appears to be associated with a velocity-dependent vanishing of the coupling between the incident antikink and the boundary mode. It would be very interesting to develop an analytical understanding of this phenomenon, but we will leave this for future work.

Conclusions. Our investigations of the boundary ϕ^4 theory have shown that it offers a considerably richer variety of resonance phenomena than the bulk theory, but within a setting where analytical progress can be made. Key features include the modification of the force leading to the sharpening of window boundaries and the new

critical velocity v_{cr} , the resurrection of the first ‘missing’ scattering window, the observation of the boundary oscillon, and the collision-induced decay of the metastable boundary vacuum for H near to 1. Many issues remain for further study, the most pressing being the development of a reliable moduli space approximation incorporating the boundary degrees of freedom. Furthermore, we feel that this model is sufficiently simple that it offers an ideal playground for the development of better analytical techniques for the understanding of more general nonintegrable field theories.

Acknowledgements. PED would like to thank Robert Parini for discussions of related matters. His work was supported by an STFC Consolidated Grant, ST/L000407/1, and by the GATIS Marie Curie FP7 network (gatis.desy.eu) under REA Grant Agreement No 317089, while that of YS was supported by the A. von Humboldt Foundation under the Institutes Linkage Programme and by the JINR Bogoljubov-Infeld Programme.

[1] P. Fendley, Phys. Rev. Lett. **71** (1993) 2485.

[2] O.H. Olsen and M.R. Samuelsen, J. Appl. Phys. **52** (1981) 6247.

[3] F. Alcaraz, M. Barber, M. Batchelor, R. Baxter and

G. Quispel, J. Phys. A **20** (1987) 6397.

[4] C.L. Kane and M.P.A. Fisher, Phys. Rev. B **46** (1992) 15233.

[5] S. Ghoshal and A.B. Zamolodchikov, Int. J. Mod. Phys. A **9** (1994) 3841 [Erratum-ibid. A **9** (1994) 4353]

[6] P. Bowcock, E. Corrigan, P.E. Dorey and R.H. Rietdijk, Nucl. Phys. B **445** (1995) 469.

[7] V.A. Rubakov, JETP Lett. **33** (1981) 644 [Pisma Zh. Eksp. Teor. Fiz. **33** (1981) 658].

[8] X.G. Wen, Phys. Rev. B **41** (1990) 12838.

[9] N.D. Antunes, E.J. Copeland, M. Hindmarsh and A. Lukas, Phys. Rev. D **69** (2004) 065016.

[10] D.K. Campbell, J.F. Schonfeld and C.A. Wingate, Physica **9D** (1983) 1.

[11] M. Peyrard and D.K. Campbell, Physica **9D** (1983) 33.

[12] P. Anninos, S. Oliveira and R.A. Matzner, Phys. Rev. D **44** (1991) 1147.

[13] R. Goodman and R. Haberman, Phys. Rev. Lett. **98** (2007) 104103.

[14] P. Dorey, K. Mersh, T. Romanczukiewicz and Y. Shnir, Phys. Rev. Lett. **107** (2011) 091602.

[15] I.L. Bogolyubsky and V.G. Makhankov, JETP Lett. **24** (1976) 12.

[16] T. Romanczukiewicz and Y. Shnir, Phys. Rev. Lett. **105** (2010) 081601.

[17] T. Sugiyama, Prog. Theor. Phys. **61** (1979) 1550.

[18] N.S. Manton and H. Merabet, Nonlinearity **10** (1997) 3.

[19] T. Romanczukiewicz, J. Phys. A **39** (2006) 3479.